Uncertainty in local determination of anisotropy parameters from a walkaway VSP

Ellen S. Gomes [1], Ivan Pšenčík [2], Greg Ball [3]

[1] Universidade Federal de Pará, Av.Tavares Bastos, 1485 Bloco 15, Belém, Pará, 66615-005, Brazil. E-mail ellensg@ufpa.br
[2] Geophysical Institute, Acad. Sci. of Czech Republic, Boční II, 141 31 Praha 4, Czech Republic. E-mail: ip@ig.cas.cz
[3] Chevron U.S.A. Inc., 6001 Bollinger Canyon Road, Bldg. 6, SanRamon, CA 94583, U.S.A. E-mail: greg.ball@chevron.com

Summary

A walkaway VSP consisting of four walkaway lines at three different VSP tool depths is analyzed to estimate the uncertainty in the local determination of anisotropy parameters. The estimated polarizations and vertical slownesses from wavefield separation for down-going and up-going compressional waves incident at the eight 3-component geophones in the VSP tool are used in the analysis. The analysis is performed assuming isotropy, transverse isotropy with a vertical symmetry axis, and general anisotropy. For the walkaway line with the best data quality, the analysis clearly shows that the shale in which the VSP tool is placed is anisotropic and that the symmetry axis is inclined from vertical. Nevertheless, the uncertainty in the estimates of the anisotropy parameters is large. The most reliably determined parameter is the compressional-wave velocity along the symmetry axis. The analysis shows the competing effects of adding the reflected up-going compressional waves in the analysis and the level of noise in these data.

Keywords: weak anisotropy, P waves, slowness vector, polarization vector, local inversion, walkaway VSP.

1 Introduction

A description of seismic anisotropy in the overburden is necessary for accurate seismic imaging, reflection amplitude analysis, and the correction of borehole sonic logs. A walkaway VSP provides an opportunity to perform a macroscopic determination of anisotropy

Seismic Waves in Complex 3-D Structures, Report 17, (Department of Geophysics, Faculty of Mathematics and Physics, Charles University, Praha 2007), pp.63-77

parameters in the overburden through an analysis of total travel times from sources to receivers and also to perform a local determination of anisotropy parameters of the formation in which the VSP tool is placed using measured polarizations and slownesses. This paper focuses on the uncertainty in the local determination of anisotropy parameters, as described in Gomes et al. (2004). One aspect of the local determination is whether the uncertainty is reduced by including information on reflected up-going compressional waves where the primary data consists of information on the down-going compressional waves. In a study on synthetic data, Gomes et al. (2004) concluded that including the up-going data has a stabilizing effect on the inversion. Nevertheless, this conclusion is dependent on the level of noise assumed to exist in the data.

This paper focuses on addressing the uncertainty in anisotropy parameter estimation using a real VSP and the value of including up-going arrivals. The walkaway VSP was acquired for three different placements in depth of the VSP tool. For each placement, the VSP tool contained eight 3-component geophones separated by 15 m. For the deepest placement, one walkaway line (Line 1) was acquired in the geologic strike direction and a second line (Line 2) was acquired in the geologic dip direction. For the middle placement (Line 3) and the shallowest placement (Line 4), lines were acquired only in the geologic dip direction. The walkaway lines are sufficiently long that arrivals from the farthest shots are traveling near horizontal when recorded by the VSP tool. The three VSP tool placements were in massive homogeneous shales. The geologic dip of the shales reaches approximately 30 degrees at the deepest VSP tool placement. Laboratory velocity measurements on shale cored in the well in the vicinity of the deepest VSP tool placement indicate large anisotropy and a direction of the symmetry axis perpendicular to the dip of the shales. From a wavefield separation performed previously for each walkaway line, polarizations and vertical slownesses are available for down-going and up-going compressional waves as well as for down-going and up-going shear waves.

2 Data

P-wave data from four lines of the VSP experiment are available for the local determination of anisotropy at three systems of receivers situated at diferent depths. The data consist of vertical components of the slowness vectors and of polarization vectors generated by shots along surface profiles and recorded at the receivers. The original feet were transformed into meters. The observed data are displayed in Figs. 2-7 below in the form used in Fig.2 of Gomes et al. (2004): vertical components of the slowness vectors (in s/km) are plotted as functions of polarization angles (in degrees), i.e., angles between the polarization vector and the vertical. The polarization angles are positive in the clockwise direction from the polarization vector to the vertical pointing down as shown in Fig.1.

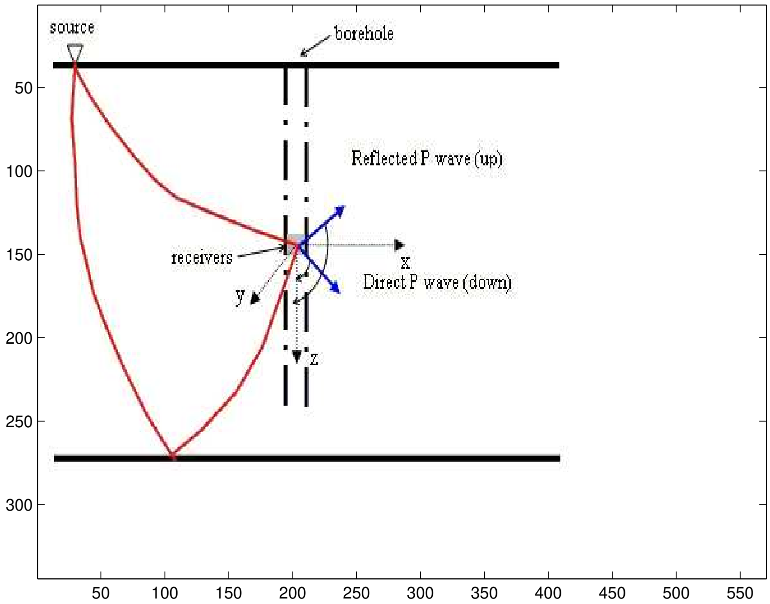

Fig. 1 Experiment configuration. Red: rays of down- and upgoing waves, blue: polarization vectors.

The data set WA1 was acquired in the geologic strike direction. The strike profile was at an azimuth of 60^0 west of North, with the receiver at depth of 4308.51m and with 266 shots. Fig.2 shows data for direct P wave (red), reflected P wave (blue), direct S wave (green) and reflected S wave (light blue).

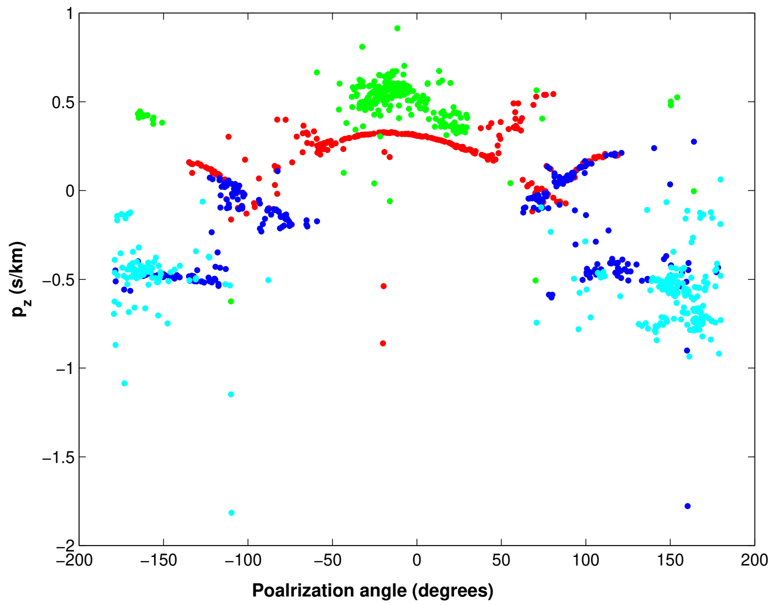

Fig. 2 WA1 data set. Direct P wave (red), reflected P wave (blue), direct S wave (green) and reflected S wave (light blue) for the receiver at 4308.51m.

The data set WA2 was acquired in the geologic dip direction. The dip profile was at an azimuth of 30^0 east of North, with the receiver at depth of 4308.51m and with 382 shots. Fig.3 shows data for direct P wave (red), reflected P wave (blue), direct S wave (green) and reflected S wave (light blue).

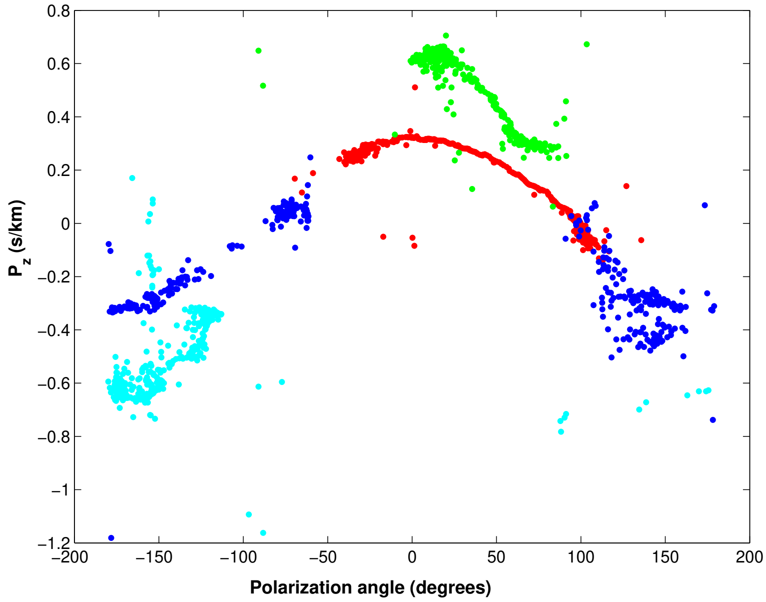

Fig. 3 WA2 data set. Direct P wave (red), reflected P wave (blue), direct S wave (green) and reflected S wave (light blue) for the receiver at 4308.51m.

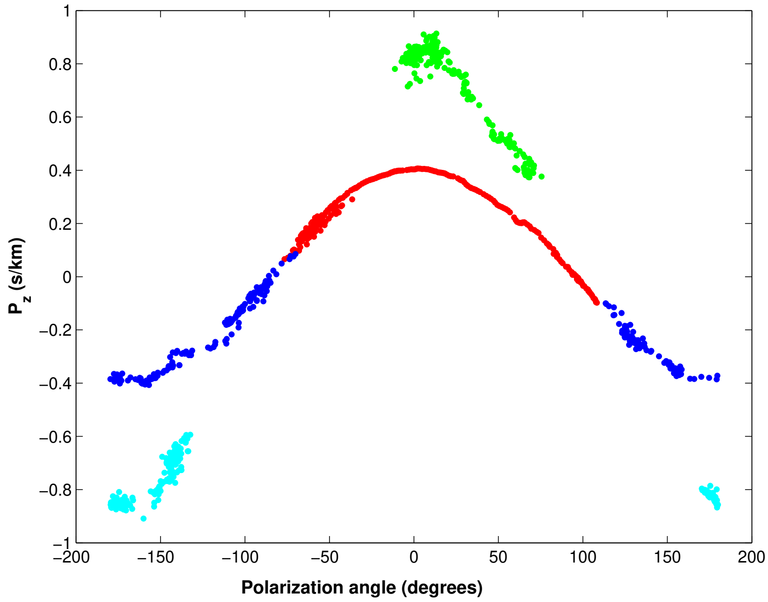

Fig. 4 WA3 data set. Direct P wave (red), reflected P wave (blue), direct S wave (green) and reflected S wave (light blue) for the receiver at 3197.08m.

The data set WA3 was acquired in the geologic dip direction. The dip profile was at an azimuth of 30^0 east of North, with one receiver, R1, at the depth of 3197.08m and another, R2, at the depth of 3212.16m, with 252 shots. Figs.4 and 5 show data for direct P wave (red), reflected P wave (blue), direct S wave (green) and reflected S wave (light blue) corresponding to the receivers R1 and R2, respectively.

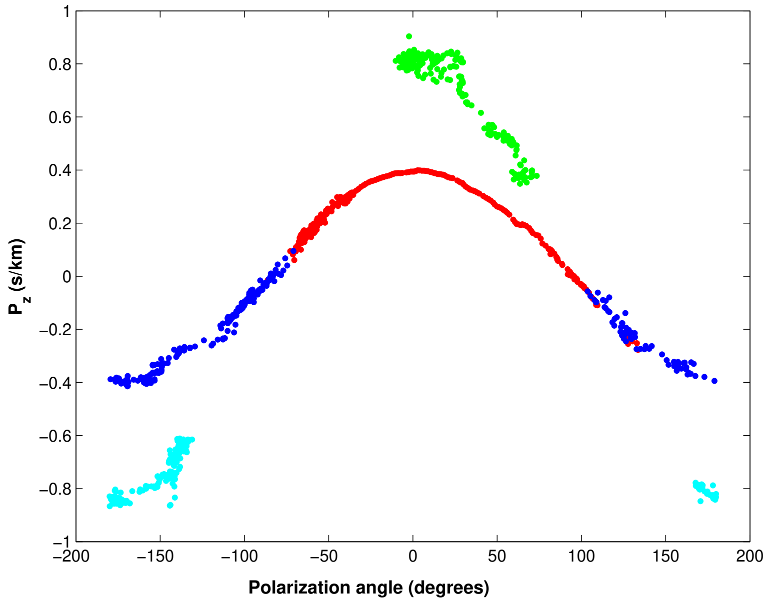

Fig. 5 WA3 data set. Direct P wave (red), reflected P wave (blue), direct S wave (green) and reflected S wave (light blue) for the receiver at 3212.16m.

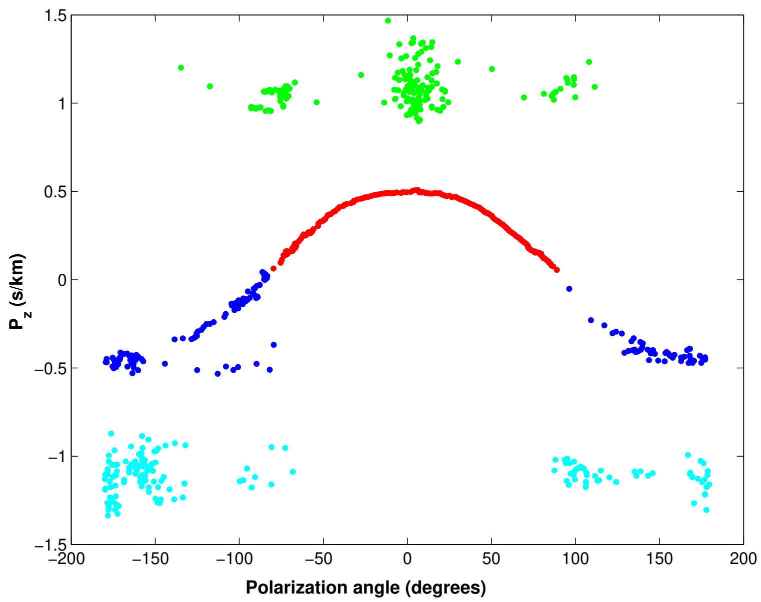

Fig. 6 WA4 data set. Direct P wave (red), reflected P wave (blue), direct S wave (green) and reflected S wave (light blue) for the receiver R1 at 2438.28m.

The data set WA4 was obtained along the "dip" profile. The dip line was at an azimuth of 30^0 east of North, with one receiver, R1, at the depth of 2438.28m and another, R2, at the depth of 2453.40m, with 165 shots. Figs.6 and 7 show data for direct P wave (red), reflected P wave (blue), direct S wave (green) and reflected S wave (light blue) corresponding to the receivers R1 and R2, respectively.

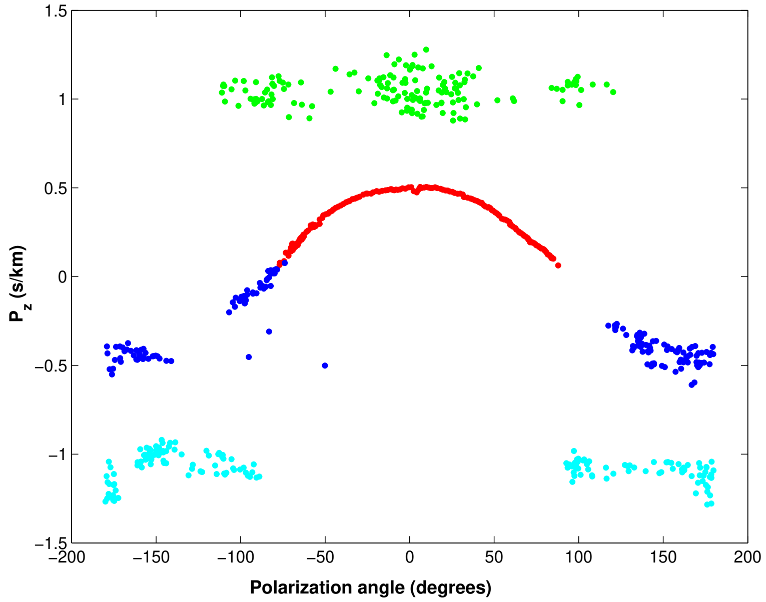

Fig. 7 WA4 data set. Direct P wave (red), reflected P wave (blue), direct S wave (green) and reflected S wave (light blue) for the receiver R2 at 2453.40m.

It can be seen that the best quality data are from the data set WA3. Slightly lower, especially for upgoing waves, is the quality of the data set WA4. Data sets WA1 and WA2 do not seem suitable for the inversion. In the following, we concentrate on the WA3 data set. An attempt ot invert the data set WA4 has also been made, its results will be reported later.

3 Inversion - WA3 data set

The inversion consists of two steps. In the first step, inversion scheme of Gomes et al. (2004) is used to find the parameters of the medium related to the global coordinate system with the z-axis vertical and x- and y-axes horizontal. In the second step, the angle of inclination θ of the axis of symmetry of the assumed TI medium is first estimated, then used to determine the parameters of the medium related to the local coordinate system with the axis of symmetry serving as the axis z.

3.1 First step: Inversion assuming isotropy, VTI symmetry, and general anisotropy

The inversion scheme of Gomes et al. (2004) was used for the inversion. Only direct (downgoing) and reflected (upgoing) P waves were considered. To avoid distortion of the results of inversion, no weighting was used, i.e., $w_i = 1$ in Eq.(7) of Gomes et al. (2004). Inversion was performed for both receivers, for which the data are shown in Figs.4 and 5. Three types of inversion were performed as in Gomes et al. (2004). We assumed successively that the studied medium is isotropic (ISO inversion), VTI (VTI inversion) and of general anisotropy (ANI inversion). Since data along a single profile are only available, it means that only parameters A_{11}, A_{33} and $A_{13} + 2A_{55}$ can be found during the VTI inversion and two additional parameters, A_{15} and A_{35}, in the case of the ANI inversion. To find the remaining parameters, data from additional profiles with different azimuths and data of S waves should be used.

A reference isotropic velocity α was determined as a least-square solution of the relation

$$\alpha p_z^{(i)} = g_z^{(i)}. \tag{1}$$

Here $p_z^{(i)}$ and $g_z^{(i)}$ are $z-$components of the slowness and polarization vectors, respectively, generated by the ith shot. For each shot, the unit wave-normal vector $\mathbf{n}$ in the reference medium, which is also necessary for the inversion, was chosen as parallel to the observed polarization vector $\mathbf{g}$.

The results of the inversion for the receivers R1 and R2 situated at the depths of 3197.08m and 3212.16m are shown in Tables 1 and 2, respectively. The parameters $A_{\alpha\beta}$ are density-normalized elastic parameters. The inversion was made for the WA parameters as in Gomes et al. (2004). The estimates of WA parameters and of their variations were then converted into the estimates of elastic parameters and their variations shown in Tables 1 and 2. For the determination of standard deviations (variations) of individual estimated parameters knowledge of the standard deviations of errors of the observed data was necessary. Since they were not known, we estimated them from the RHS of Eq.(7) of Gomes et al. (2004) with unit weights w_i, divided by the number of data points N. We assumed that the distribution of errors in the data was Gaussian, see Beck and Arnold (1976) or Menke (1984). We can see that the parameters with the smallest variations are parameters A_{33} (in both ANI and VTI experiments) and A_{15} and A_{35}.

Tables 1 and 2 show an interesting difference of values of elastic parameters in receivers separated by only 15m. Vertical velocities are slightly larger and horizontal velocities considerably lower for the deeper receiver. This might be either an indication of rapid variation of geological conditions or an indication that the assumption of Gaussian distribution of errors of data is not apropriate. Another interesting observation is the size of misfit, which is 100-times less than in the case of data used by Gomes et al. (2004). This indicates the high quality of the WA3 data set. A worse misfit was found for the data set WA4. It is also interesting that the velocities at the depth of 3km are relatively small, between 2.0 and 3.0 km/s.

	Estimate of α	Misfit	Elastic parameters	Estimated values	Variation
ISO	2.52	8.27E-02	A_{33}	6.31	(6.24 6.39)
VTI			A_{11}	3.35	(1.92 4.80)
	2.51	8.23E-02	A_{33}	6.10	(5.97 6.24)
			$A_{13} + 2A_{55}$	4.16	(3.14 5.18)
ANI			A_{11}	6.22	(5.53 6.92)
			A_{33}	6.27	(6.20 6.34)
	2.51	3.95E-02	$A_{13} + 2A_{55}$	6.04	(5.55 6.54)
			A_{15}	-0.48	(-0.49 -0.46)
			A_{35}	-0.38	(-0.40 -0.36)

Tab. 1 Results of inversion for receiver R1 of the WA3 data set.

	Estimate of α	Misfit	Elastic parameters	Estimated values	Variation
ISO	2.56	7.82E-02	A_{33}	6.54	(6.47 6.61)
VTI			A_{11}	2.80	(1.37 4.24)
	2.56	7.77E-02	A_{33}	6.23	(6.10 6.40)
			$A_{13} + 2A_{55}$	3.93	(2.92 4.96)
ANI			A_{11}	5.14	(4.37 5.92)
			A_{33}	6.37	(6.30 6.45)
	2.56	4.12E-02	$A_{13} + 2A_{55}$	5.41	(4.86 5.97)
			A_{15}	-0.47	(-0.47 -0.45)
			A_{35}	-0.33	(-0.35 -0.31)

Tab. 2 Results of inversion for receiver R2 of the WA3 data set.

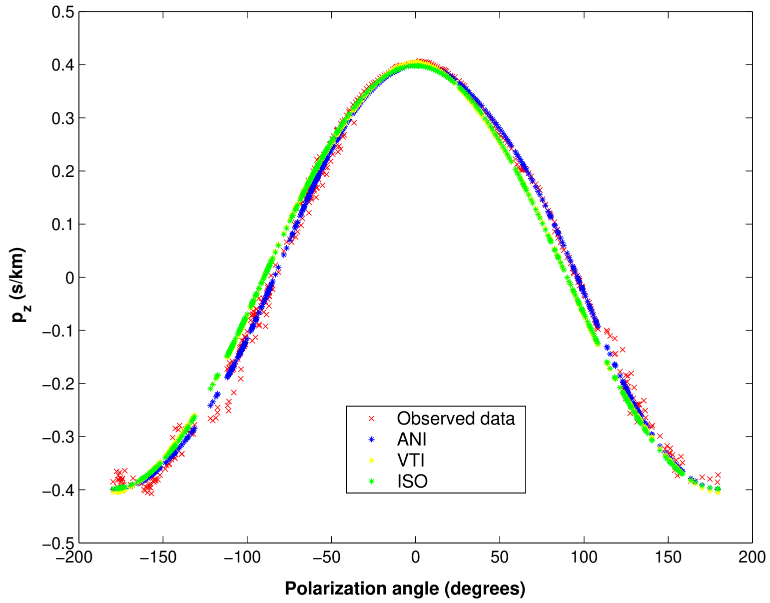

Fig. 8 WA3 data set, receiver R1. Vertical component of the slowness vector p_z in s/km as a function of polarization angle (in degrees). Red crosses: observed data; green dots: ISO inversion; yellow dots: VTI inversion; blue dots: ANI inversion.

Figs. 8 and 9 show comparison of the observed data with synthetic data corresponding to the estimated parameters shown in Tabs. 1 and 2 for receivers R1 and R2, respectively. Figs. 8 and 9 show again the vertical components of the slowness vector, p_z, as functions of the polarization angles in degrees. The observed data are denoted by red crosses, the

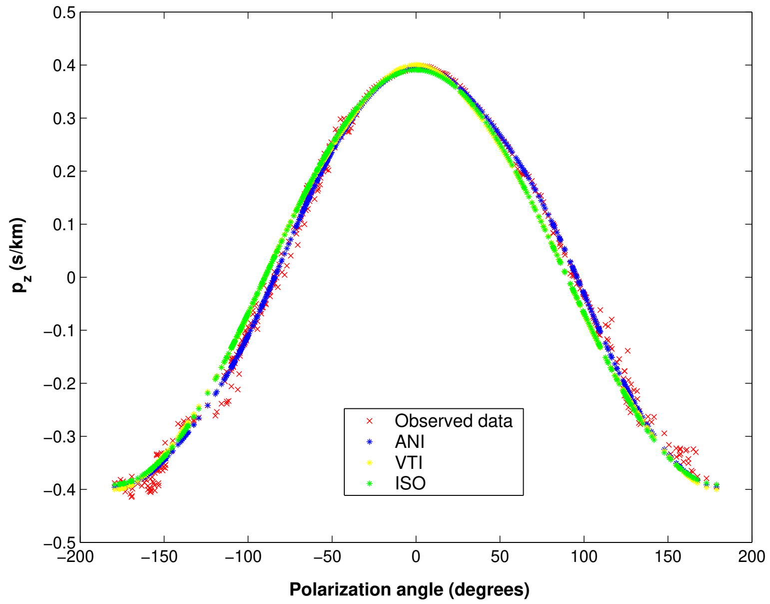

Fig. 9 WA3 data set, receiver R2. Vertical component of the slowness vector p_z in s/km as a function of polarization angle (in degrees). Red crosses: observed data; green dots: ISO inversion; yellow dots: VTI inversion; blue dots: ANI inversion.

data obtained for ISO inversion by green dots, for VTI inversion by yellow dots and for the ANI inversion by blue dots. Although there are differencies between various types of inversion (ISO, VTI, ANI), they are difficult to be identified.

In order to increase the differences between individual types of inversion, we show the results in the form of the dependence of the quantity $\alpha p_z/g_z$ on the polarization angle, again for the receivers R1 and R2, see Figs. 10 and 11. The notation is the same as in

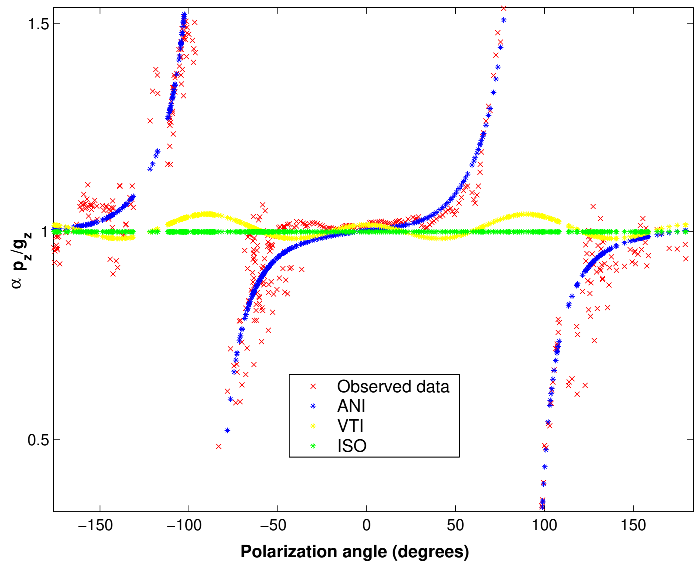

Fig. 10 WA3 data set, receiver R1. The non-dimensional quantity $\alpha p_z/g_z$ as a function of polarization angle (in degrees). Red crosses: observed data; green dots: ISO inversion; yellow dots: VTI inversion; blue dots: ANI inversion.

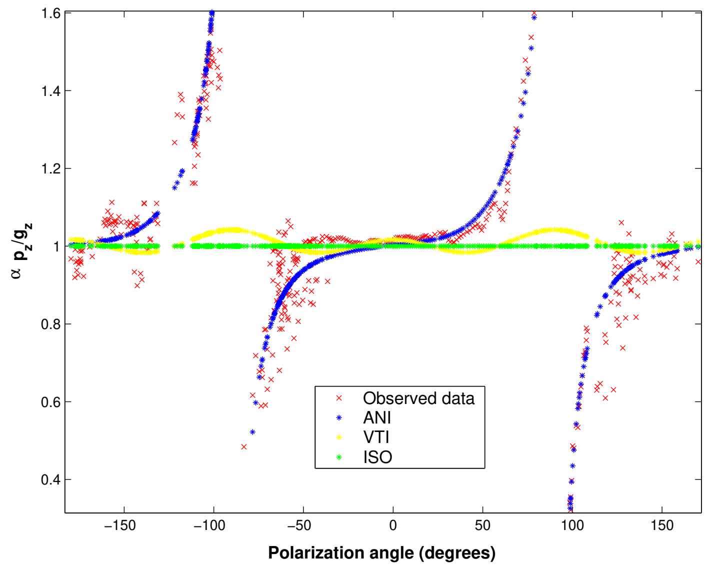

Fig. 11 WA4 data set, receiver R2. The non-dimensional quantity $\alpha p_z/g_z$ as a function of polarization angle (in degrees). Red crosses: observed data; green dots: ISO inversion; yellow dots: VTI inversion; blue dots: ANI inversion.

Figs.8 and 9. We can see very well that data corresponding to the ISO and VTI inversions form a horizontal line or oscillate around it, and ignore the real data (red). On the other hand, the data corresponding to ANI inversion aproximate the observed data very well. There is no doubt that we should work only with ANI results in the next step.

3.2 Second step: TI inversion assuming a tilted axis of symmetry

From the geological description of the medium around the receivers we know that it is formed by shale. This means that we can expect TI symmetry with, very probably, tilted axis of symmetry. Therefore, we seek first the orientation of the axis of symmetry of a TI medium. Our task simplifies since, according to the description, the profile, along which the data set WA3 was observed, runs along the dip of the geological formation. It means that we can consider the azimuth of the plane containing the axis of symmetry to be known and equal zero. It thus remains to find the angle of inclination of the axis of symmetry of the TI medium. When we find it, we can evaluate the elastic parameters in the local, rotated system of coordinates, in which the z-axis is parallel to the symmetry axis. In order to distinguish the parameters in the local coordinate system from the parameters $A_{\alpha\beta}$ in the global one, we mark them by prime: $A'_{\alpha\beta}$. Because the medium in which the VSP tool is placed is a shale, we expect that $A'_{11} > A'_{33}$.

We have thus based the second step of the inversion on three assumptions: i) the studied medium is TTI; ii) the azimuth of the axis of symmetry is zero and we seek only the agle of inclination θ; iii) $A'_{11} > A'_{33}$.

Let us specify the orientation of the axis of symmetry of TI medium by an angle θ, made by the axis of symmetry and the positive x-axis; θ being positive when measured clockwise. With the above three assumptions in mind, the angle θ can be found from formula

$$\tan 2\theta = \frac{2(A_{15} + A_{35})}{A_{33} - A_{11}}. \tag{2}$$

Eq.(2) follows from the well-known formula for the transformation of the tensors of the fourth rank

$$a'_{i'j'k'l'} = c_{i'i}c_{j'j}c_{k'k}c_{l'l}a_{ijkl}. \tag{3}$$

Eq.(2) yields two angles, θ and $\theta + \frac{\pi}{2}$. To choose the proper angle, we use the assumption iii), see above. In order to find the estimates of the angle θ and of the elastic parameters in the local coordinate system and their variations, we used eq. (2) for the determination of θ and eq. (3) for the determination of A'_{11}, A'_{33}, $A'_{13} + 2A'_{55}$, A'_{15} and A'_{35} for values of A_{11}, A_{33}, A_{15} and A_{35} varying in the intervals shown in the last columns of Tabs.1 and 2. In this way, we generated 100,000 values of the studied parameters, from which we estimated values of parameters shown in Tabs. 3 and 4 and their variations for the receivers R1 and R2, respectivelly.

For the receiver R1, the angle θ was found to be 45.74^0, and to vary in the interval ($33.34^0 \quad 58.02^0$). For the receiver R2, the angle θ was estimated as 63.07^0 and varying within the interval ($51.44^0 \quad 72.05^0$). For Thomsen's (1986) parameter

$\epsilon = (A'_{11} - A'_{33})/2A'_{33}$, Table 3 yields ϵ =0.17, which may vary in interval (0.15 0.21). Similarly, for the receiver R2, see Tab.4, we get ϵ =0.23, which may vary in the interval (0.15 0.35). Note the differences in definitions of ϵ above and $\epsilon_x = (A_{11} - \alpha^2)/2\alpha^2$ and $\epsilon_z = (A_{33} - \alpha^2)/2\alpha^2$, where α is given in Tabs. 1 and 2.

3.3 Effects of upgoing waves

The large difference between the angles θ for the receivers R1 (45.74^0) and R2 (63.07^0), which are separated by only 15m depth lead us to the study of effects of upgoing waves on the inversion based on the use of the data from both downgoing and upgoing waves. Gomes et al. (2004) studied this problem on synthetic data and came to the conclusion that use of the data of the upgoing waves has a stabilizing effect on the inversion. Although Gomes et al. (2004) considered the errors of the data of the upgoing waves to be larger than those of the downgoing waves, it is possible that they were, nevertheless, underestimated. From this reason, further studies of inversion of synthetic data are planned.

In order to estimate effects of upgoing waves on the results of inversion, we made the following experiments. In addition to results shown in Tabs.3 and 4, for which both down- and upgoing waves were used, we also made inversions for both receivers separately for down- and upgoing waves.

The results for the receiver R1 are shown in Tab.5 (downgoing waves) and Tab.6 (upgoing waves). Rotation angle θ for the inversion based on data from only downgoing waves was estimated to be 67.43^0, with variation between 58.15^0 and 74.37^0. Corresponding Thomsen's parameter ϵ was estimated as 0.28 with variation in the interval (0.18 0.43). Rotation angle θ for the inversion based on upgoing waves only was estimated to be 24.92^0, with variation between 16.09^0 and 36.95^0. The Thomsen's parameter ϵ was estimated as 0.23 with variation between 0.17 and 0.30.

The same experiment made for the receiver R2 yielded the following results (the corresponding elastic and WA parameters after rotation are not shown here). Rotation angle θ for the inversion based on data from only downgoing waves was estimated to be 56.52^0, with variation between 42.79^0 and 68.15^0. Corresponding Thomsen's parameter ϵ was estimated as 0.15 with variation in the interval (0.11 0.22). Rotation angle θ for the inversion based on upgoing waves only was estimated to be 72.16^0, with variation between 61.79^0 and 78.86^0. The Thomsen's parameter ϵ was estimated as 0.66 with variation between 0.26 and 1.38.

When only data from downgoing waves are used, we can see that the angles θ for the receivers R1 (67.43^0) and R2 (56.52^0) are now closer to each other than in the case of use of both down- and upgoing waves. The variation of the angle θ for the receiver R1 is smaller when only the downgoing wave is used than when both waves are used. For the receiver R2, it is, however, just opposite. Resulting values of the Thomsen's parameter ϵ, when only downgoing waves are used, differ for both receivers even more than when both waves are used. Thus, the use of data of only downgoing waves seems to only lead to more consistent estimates of the angle θ for both receivers. From the above comparison,

Elastic parameters	Estimated values	Variation
A'_{11}	7.04	(6.59 7.56)
A'_{33}	5.26	(4.74 5.74)
$A'_{13}+2A'_{55}$	6.34	(6.03 6.60)
A'_{15}	2.9E-02	(-5.4E-02 7.6E-02)
A'_{35}	-2.9E-02	(-7.6E-02 5.4E-02)

WA parameters	Estimated values	Variation
ϵ_x	5.9E-02	(2.3E-02 0.1)
ϵ_z	-8.3E-02	(-0.12 -4.4E-02)
δ_x	5.6E-03	(-4.4E-02 4.8E-02)
ϵ_{15}	4.7E-03	(-8.6E-03 1.2E-02)
ϵ_{35}	-4.7E-03	(-1.2E-02 8.6E-03)

Tab. 3 Elastic and WA parameters in the local coordinate system for receiver R1 of the WA3 data set. Rotation angle θ=45.74^0, its variation (33.34^0 58.02^0).

Elastic parameters	Estimated values	Variation
A'_{11}	6.63	(6.40 6.93)
A'_{33}	4.57	(3.88 5.24)
$A'_{13}+2A'_{55}$	5.90	(5.29 6.42)
A'_{15}	-6.0E-02	(-0.16 -6.4E-02)
A'_{35}	6.0E-02	(-6.4E-02 0.16)

WA parameters	Estimated values	Variation
ϵ_x	5.5E-03	(-1.2E-02 2.9E-02)
ϵ_z	-0.15	(-0.20 -0.10)
δ_x	-0.10	(-0.19 -2.0E-02)
ϵ_{15}	-9.1E-03	(-2.4E-02 9.8E-03)
ϵ_{35}	9.1E-03	(-9.8E-03 2.4E-02)

Tab. 4 Elastic and WA parameters in the local coordinate system for receiver R2 of the WA3 data set. Rotation angle θ=63.07^0, its variation (51.44^0 72.05^0).

Elastic parameters	Estimated values	Variation
A'_{11}	6.16	(6.00 6.37)
A'_{33}	3.96	(3.32 4.60)
$A'_{13}+2A'_{55}$	5.40	(4.81 5.97)
A'_{15}	-9.1E-02	(-0.18 2.7E-02)
A'_{35}	9.1E-02	(-2.7E-02 0.18)

WA parameters	Estimated values	Variation
ϵ_x	-1.9E-02	(-3.2E-02 -2.6E-03)
ϵ_z	-0.19	(-0.24 -0.14)
δ_x	-0.16	(-0.25 -6.7E-02)
ϵ_{15}	-1.4E-02	(-2.8E-02 4.2E-03)
ϵ_{35}	1.4E-02	(-4.2E-03 2.8E-02)

Tab. 5 Elastic and WA parameters obtained from the down-going wave in the local coordinate system for the receiver R1 of the WA3 data set. Rotation angle θ=67.43^0, its variation (58.15^0 74.37^0).

Elastic parameters	Estimated values	Variation
A'_{11}	8.90	(7.92 9.91)
A'_{33}	6.13	(5.73 6.44)
$A'_{13}+2A'_{55}$	7.55	(6.80 8.36)
A'_{15}	-5.6E-02	(-0.13 3.0E-02)
A'_{35}	5.6E-02	(-3.0E-02 0.13)

WA parameters	Estimated values	Variation
ϵ_x	0.21	(0.13 0.29)
ϵ_z	-9.9E-03	(-4.2E-02 1.5E-02)
δ_x	0.21	(8.7E-02 0.34)
ϵ_{15}	-9.0E-03	(-2.1E-02 4.8E-03)
ϵ_{35}	9.0E-03	(-4.8E-03 2.1E-02)

Tab. 6 Elastic and WA parameters obtained from the up-going wave in the local coordinate system for the receiver R1 of the WA3 data set. Rotation angle θ=24.92^0, its variation (16.09^0 36.95^0).

it is also obvious that the use of only data from upgoing waves may lead to distorted results; see, for example estimated value 0.66 of the parameter ϵ, which indicates 66% anisotropy!

4 Conclusion

Polarizations and slownesses of compressional waves for a walkaway line were inverted for the anisotropy parameters of the shale in which the VSP tool was placed. Within the uncertainty of the inversion, the appropriate description of the shale is that it exhibits transverse isotropy with axis of symmetry inclined from vertical. This description is consistent with geological and laboratory data. Inclusion of up-going compressional waves may help stabilize the inversion, but this is dependent on the noise level in the data. There might be an opportunity to reduce the uncertainty through a more accurate wavefield separation. Nevertheless, the uncertainty in the estimation of the anisotropy parameters remains large, specifically of the parameter A_{11}, which affects accuracy of the determination of the angle θ of inclination of the axis of symmetry, see eq. (2). It might be necessary to include complementary data in the inversion to significantly reduce this uncertainty.

Acknowledgement

The authors would like to thank Chevron and partners for providing the data. The authors are also grateful to consortium project "Seismic waves in complex 3-D structures"

References

Beck, J. and Arnold, K.J., 1976. *Parameter estimation.* John Wiley & sons, New York.

Gomes, E., Zheng, X., Pšenčík,I., Horne,S. and Leaney,S., 2004. Local determination of weak anisotropy parameters from a walkaway VSP qP-wave data in the Java Sea region. *Stud. Geophys. Geod.*, **48**, 215-230.

Menke, W., 1984. *Geophysical data analysis: Discrete inverse theory.* Academic Press, New York.

Thomsen,L., 1986. Weak elastic anisotropy. *Geophysics*, **51**, 1954-1966.